HHS Public Access

Author manuscript

*Neuron*. Author manuscript; available in PMC 2017 December 07.

Published in final edited form as:

*Neuron*. 2016 December 07; 92(5): 1049–1062. doi:10.1016/j.neuron.2016.10.030.

# Neural architecture of hunger-dependent multisensory decision making in *C. elegans*

**D. Dipon Ghosh**[1], **Tom Sanders**[2], **Soonwook Hong**[1], **Li Yan McCurdy**[1,3], **Daniel L. Chase**[4], **Netta Cohen**[2], **Michael R. Koelle**[5], and **Michael N. Nitabach**[1,6,7,8,9]

[1]Department of Cellular and Molecular Physiology, Yale University, New Haven, CT

[2]School of Computing, University of Leeds, Leeds LS2 9JT, United Kingdom

[3]Interdepartmental Neuroscience Program, Yale University, New Haven, CT

[4]Department of Biomolecular Sciences, Central Connecticut State University, New Britain, CT

[5]Department of Molecular Biophysics and Biochemistry, Yale University, New Haven, CT

[6]Department of Genetics, Yale University, New Haven, CT

[7]Program in Cellular Neuroscience, Neurodegeneration and Repair, Yale University, New Haven, CT

## SUMMARY

Little is known about how animals integrate multiple sensory inputs in natural environments to balance avoidance of danger with approach to things of value. Furthermore, the mechanistic link between internal physiological state and threat-reward decision making remains poorly understood. Here we confronted *C. elegans* worms with the decision whether to cross a hyperosmotic barrier presenting the threat of desiccation to reach a source of food odor. We identified a specific interneuron that controls this decision via top-down extrasynaptic aminergic potentiation of the primary osmosensory neurons to increase their sensitivity to the barrier. We also establish that food deprivation increases the worm's willingness to cross the dangerous barrier by suppressing this pathway. These studies reveal a potentially general neural circuit architecture for internal state control of threat-reward decision making.

[8]Corresponding author: michael.nitabach@yale.edu.
[9]Lead contact: michael.nitabach@yale.edu



**Author Contributions**

DDG, TS, NC, MRK, MNN designed study and experiments. DDG, SH, DLC performed experiments. TS and NC performed computational modeling. DDG, TS, LYM, DLC, NC, MRK, and MNN analyzed the data. DDG and MNN wrote the paper with input from the other authors.

**Author Information**

The authors declare no conflicts of interest.

## INTRODUCTION

Animals navigate complex natural environments containing both dangerous and valuable items, such as predators and food. The sensory cues that signal danger and reward are frequently transduced by different senses. In such circumstances, multisensory decision processes survey internal physiological state and balance attention to relevant sensory modalities to drive behavioral outputs (Rangel et al., 2008; Talsma et al., 2010). In human beings and other mammals, a key motif of multisensory integration is “top-down” control of perception (Manita et al., 2015; Talsma et al., 2010), wherein primary sensory cortex activity is modulated by feedback from higher-order regions (Fairhall and Macaluso, 2009; Fu et al., 2014; Zhang et al., 2014). Top-down control directs attention to the sensory modality signaling the most important features of a noisy environment given current internal physiological state (Berthoud, 2011; Rangel et al., 2008; Talsma, 2015). However, cellular and molecular mechanisms underlying internal state-dependent top-down attentional control in the context of threat-reward decision making remain unknown.

Here we employ the nematode worm *Caenorhabditis elegans* as a model system to investigate the molecular and cellular basis of multisensory decision making. In its natural environment in decomposing organic matter (Frezal and Felix, 2015), *C. elegans* must approach and obtain food while avoiding various threats, which include toxic chemicals and hyperosmotic concentrations of otherwise innocuous solutes. Worms detect threat and reward *via* primary sensory neurons that then propagate such information through an interneuron network to ultimately reach premotor command interneurons that direct locomotion (Figure 1A) (Varshney et al., 2011; White et al., 1986). The attractive food odor diacetyl is detected by the bilateral chemosensory neuron pair AWA (Sengupta et al., 1996). Avervise hyperosmolarity—which can induce damage and death by desiccation (Culotti and Russell, 1978; Solomon et al., 2004)—is detected by the bilateral polymodal sensory neuron pair ASH (Hilliard et al., 2005; Kaplan and Horvitz, 1993). AWA and ASH propagate their sensory responses to an interconnected network of sensory interneurons (Ishihara et al., 2002; Luo et al., 2014; Shinkai et al., 2011). These sensory interneurons then provide inputs to the bilateral pair of RIM sensorimotor interneurons (Gordus et al., 2015; Guo et al., 2009; Piggott et al., 2011; White et al., 1986). RIM receives inhibitory synaptic inputs from sensory interneurons activated by attractive odors, such as diacetyl transduced by AWA (Gordus et al., 2015; Li et al., 2012). RIM receives excitatory synaptic inputs from sensory interneurons activated by aversive stimuli, such as hyperosmolarity transduced by ASH (Guo et al., 2009; Piggott et al., 2011). RIM, in turn, provides inhibitory synaptic inputs to forward command interneurons (Kawano et al., 2011; Pirri et al., 2009) and excitatory synaptic and gap-junction-coupled inputs to backward command interneurons (Gordus et al., 2015; Guo et al., 2009). This sensorimotor network topology and the signs of its synaptic connections ensure that aversive stimuli bias the worm towards backing up and changing direction, while attractive stimuli bias the worm towards continued forward motion. ASH also directly excites backward command interneurons, thus providing an alternative parallel feedforward pathway by which it can induce avoidance of danger (Guo et al., 2009).

Previous studies have implicated the AIY sensory interneurons in setting the multisensory threat-reward decision balance of approach to the attractive odor diacetyl when confronting a

toxic $Cu^{2+}$ barrier (Ishihara et al., 2002; Shinkai et al., 2011). Specifically, HEN-1 protein secreted by AIY acts on its receptor SCD-2 in another sensory interneuron pair AIA to regulate the decision to cross the $Cu^{2+}$ barrier (Ishihara et al., 2002; Shinkai et al., 2011). Dopamine also regulates this threat-reward decision (Wang et al., 2014). While food deprivation increases threat tolerance in this multisensory decision, the HEN-1 and dopamine receptor pathways are dispensable for this hunger effect (Ishihara et al., 2002; Wang et al., 2014). Thus, cellular and molecular mechanisms by which internal physiological state modulates threat-reward decision making in *C. elegans*, or indeed, any animal, remain unknown.

As discussed above, RIM is suitably positioned within the sensorimotor control network to regulate multisensory threat-reward decision making. RIM expresses the neuropeptide Pigment Dispersing Factor-2 (PDF-2) and its cognate G protein-coupled receptor (GPCR), PDFR-1 (Flavell et al., 2013; Janssen et al., 2008; Janssen et al., 2009; Meelkop et al., 2012). While PDF-1, another ligand of PDFR-1, has recently been shown to play a role in arousal-related behaviors (Barrios et al., 2012; Choi et al., 2013; Flavell et al., 2013), PDF-2 function is not well characterized. We found that PDFR-1 activation by PDF-2 in RIM decreases threat tolerance in the multisensory decision task. Unexpectedly, RIM does not control the decision via its known synaptic connections within the sensorimotor control network. Rather, RIM controls the decision by previously unknown extrasynaptic top-down tyraminergic positive feedback onto the primary osmosensory ASH neurons. Our results also indicate that internal hunger state suppresses this positive feedback loop, thereby increasing threat tolerance of food-deprived worms. These studies reveal underlying molecular and cellular mechanisms of internal state control of multisensory threat-reward decision making in the worm, and suggest that top-down topological motifs of multisensory integration are similar in mammals and the vastly simpler worm.

## RESULTS

### Hunger modulates multisensory threat-reward decision making

To provide a controlled behavioral context for exploring mechanisms underlying multisensory decision making, we employed a task in which worms balance danger of osmotic dessication with reward of food. A 1 cm diameter hyperosmotic fructose barrier ring is applied to a 5 cm diameter agar plate without food, and two 1 μL spots of diluted diacetyl food odor are applied outside the ring (Figure 1B). After allowing five minutes for the hyperosmotic solution to absorb into the agar and diffuse to establish an osmotic gradient, ten worms are removed from food-containing plates and placed in the center of the ring (Figure 1B). The decision balance between retreating from versus exiting the barrier ring is quantified as the fraction of worms that exit the ring within 15 minutes of being placed.

Approximately 30% of worms exit a 2 M fructose ring in the absence of food odor (Figure 1C), driven by their intrinsic propensity to disperse (Culotti and Russell, 1978; Gray et al., 2005). The presence of two 1 μl drops of 1:350 dilution of diacetyl in water outside the ring increases exiting to 80% (Figure 1C). This increase in exiting is abolished in *odr-10* null-mutant worms that lack the ODR-10 diacetyl receptor (Sengupta et al., 1996) (Figure 1C). Spots of more diluted diacetyl result in smaller increases in exiting (data not shown).

Increasing the fructose ring concentration to 3 M abolishes exiting even in the presence of food odor (Figure 1D). To determine if internal physiological state modulates this multisensory threat-reward decision, we deprived worms of food before testing. The decisions of worms deprived of food for fifteen minutes are indistinguishable from those of non-deprived worms (Figure 1D). In contrast, worms deprived of food for one hour increase exiting relative to non-deprived worms, and worms deprived of food for five hours increase exiting even further (Figure 1D).

## PDF-2 neuropeptide regulates multisensory decision making

As discussed above, the position of RIM in the sensorimotor control network is suitable for controlling multisensory threat-reward decision making (Figure 1A). While multiple neurons express either PDF-2 or its receptor PDFR-1, RIM expresses both (Figure 2A). PDF-1 and PDFR-1 null-mutant worms exhibit locomotor defects (Janssen et al., 2008; Meelkop et al., 2012) attributable to altered arousal state (Barrios et al., 2012; Choi et al., 2013; Flavell et al., 2013) that preclude testing in the multisensory decision assay. However, *pdf-2* null-mutant worms exhibit grossly normal locomotion (see below), allowing us to test whether the balance of threat-reward decision making is altered in *pdf-2* null-mutant worms. While wild-type worms readily exit a 2 M fructose ring to approach the source of food odor, they are almost completely contained by a 3 M ring (Figure 2B). In contrast, *pdf-2* null-mutant worms readily exit the 3 M ring to approach the source of food odor, although they are still contained by a 4 M ring (Figure 2B). Complete rescue of the wild-type decision balance by transgenic re-expression of *pdf-2* under the control of its own promoter sequence establishes the absence of PDF-2 peptide as the cause of the *pdf-2* null-mutant decision phenotype (Figure 2B). Interestingly, the *pdf-2* null mutation has no effect on avoidance of the osmotic ring in the absence of diacetyl, nor on attraction to diacetyl in the absence of the osmotic ring (Figure 2B, C, D). This absence of unisensory defects rules out primary sensory defects and suggests a specific role for PDF-2 in multisensory decision making.

To determine whether the *pdf-2* null mutation causes a general defect in locomotion in the multisensory decision paradigm, we used automated worm tracking to directly measure locomotor kinematics as worms navigate within the osmotic ring (Figure 2E). The radial distribution of *pdf-2* null-mutant worm trajectories was quantified during the first five minutes of the assay (before any *pdf-2* null-mutant worms exit the ring). Trajectories of *pdf-2* null-mutant worms are indistinguishable from wild-type worms (Figure 2F). There is also no detectable effect of the *pdf-2* null mutation on standard locomotor kinematic parameters, including reversal frequency, high angle “omega turn” frequency, reversal magnitude, and forward bout duration (Figure S1B). Exiting in the absence of food odor is unaffected in *pdf-2* null-mutant worms (Figure 2B, C), and there is no statistically significant effect of the *pdf-2* null mutation on locomotor kinematics within the ring in this unisensory context (Figure S1C, D). Taken together, these results indicate that a general defect in locomotion—such as might prevent reversal and retreat upon approaching the hyperosmotic ring—cannot account for the altered multisensory decision balance of *pdf-2* null-mutant worms.

## PDF-2 acts on PDFR-1 in RIM to set the threat-reward decision balance

We next sought to determine both the cellular origin and target site of action of PDF-2 in regulating the threat-reward decision. Targeted re-expression of *pdf-2* in *pdf-2* null-mutant worms using a promoter specific to RIM and RIC, another interneuron pair near RIM in the anterior nerve ring (White et al., 1986), fully rescues the multisensory decision (Figure 3A). While only RIM normally expresses PDF-2 (Janssen et al., 2009), this indicates that PDF-2 secretion by RIM and RIC is sufficient to mediate wild-type decision balance. To determine the relevant PDFR-1-expressing targets of PDF-2, we employed membrane-tethered PDF-2 peptide (t-PDF-2) to activate PDFR-1 in specific neurons (Figure 3B). This approach has been extensively validated *in vitro* and *in vivo* for cell-autonomous pharmacologically specific sustained activation of *Drosophila* PDFR and other class B1 neuropeptide receptors (Choi et al., 2012; Choi et al., 2009; Fortin et al., 2009; Krupp et al., 2013; Kunst et al., 2014). As noted earlier, RIM also expresses the PDF-2-receptor PDFR-1. Expression of t-PDF-2 in *pdf-2* null-mutant worms using either of two promoters whose expression overlaps solely in RIM fully rescues the decision balance (Figure 3C). Expression of t-PDF-2 in RIC, which does not express PDFR-1 (Barrios et al., 2012; Flavell et al., 2013; Janssen et al., 2008), and expression of a sequence-scrambled version of the tethered peptide (t-SCR) in RIM each fail to rescue the decision phenotype (Figure 3C). This confirms the cell-autonomy and pharmacological specificity of t-PDF-2 activation of PDFR-1 in RIM. Finally, expression of t-PDF-2 in RIM and RIC in a wild-type background does not suppress exiting of a 2 M fructose ring in the presence of diacetyl, suggesting that the PDF-2-PDFR-1 autocrine loop is maximally active in this state, thereby precluding any gain-of-function t-PDF-2 effect (Figure S2). Taken together, these data indicate that PDF-2 secretion by RIM and RIC and autocrine action of PDF-2 on PDFR-1 in RIM are each sufficient to mediate a wild-type decision balance, and establish RIM as a key locus of control of multisensory decision making in the worm.

## Tyraminergic positive feedback from RIM to ASH sets the threat-reward decision balance

How does PDFR-1 activation in RIM decrease threat tolerance in the approach to food? One way in which RIM communicates with its downstream targets is *via* secretion of the biogenic amine tyramine, which is synthesized from tyrosine in a reaction catalyzed by the enzyme tyrosine decarboxylase (TDC), encoded by the *tdc-1* gene (Figure 3D) (Alkema et al., 2005). *tdc-1* null-mutant worms lack tyramine and phenocopy the *pdf-2* null-mutant phenotype, with worms now readily exiting the 3 M ring to approach the source of food odor, and with unaltered avoidance of the osmotic ring on its own (Figure 3E). As for *pdf-2* null-mutant worms, locomotor kinematic defects do not account for the altered threat-reward decision balance of *tdc-1* null-mutant worms (Figure S1). *tdc-1* null-mutant worms also lack the biogenic amine octopamine, which is synthesized from tyramine in a reaction catalyzed by tyramine β-hydroxylase (TBH), encoded by the *tbh-1* gene (Figure 3D) (Alkema et al., 2005). However, *tbh-1* null-mutant worms, which synthesize tyramine but lack octopamine (Alkema et al., 2005), are unaffected (Figure 3E). This establishes that tyramine, and not octopamine, regulates the threat-reward decision balance. Additionally, double null-mutant *pdf-2; tdc-1* worms behave identically to both *pdf-2* and *tdc-1* single-mutant worms, suggesting that these genes function in the same genetic pathway to control the decision (Figure 3E). Finally, targeted re-expression of *tdc-1* in *tdc-1* null-mutant worms in RIM and

RIC, but not RIC alone, fully rescues the multisensory decision (Figure 3F). RIM is the only tyraminergic neuron in the sensorimotor control network (Alkema et al., 2005; Donnelly et al., 2013; Pirri et al., 2009), and the only other tyraminergic neuroendocrine cell in the worm, uv1, controls egg-laying (Alkema et al., 2005; Jose et al., 2007). Taken together with the key role of PDFR-1 activation in RIM (Figure 3C), these results strongly support the conclusion that RIM controls threat-reward decision making, and that it exerts this control *via* tyraminergic signaling to tyramine receptor-expressing targets.

What is the relevant tyramine receptor, and where and how does it act to mediate RIM control of the threat-reward decision balance? The worm genome encodes a hyperpolarizing tyramine-gated $Cl^-$ channel (LGC-55) expressed in one of the forward command interneurons, and previously shown to regulate locomotion (Pirri et al., 2009), as well as several tyramine GPCRs related to vertebrate adrenergic receptors, including TYRA-2, SER-2, and TYRA-3 (Donnelly et al., 2013; Rex and Komuniecki, 2002; Rex et al., 2004; Wragg et al., 2007). We considered LGC-55 a particularly likely target of RIM tyramine signals in the control of threat-reward decision making, as it mediates direct synaptic inhibition of forward locomotor command interneurons by RIM (Alkema et al., 2005; Pirri et al., 2009). However, the threat-reward decision balance of both *lgc-55* and *tyra-3* null-mutant worms is indistinguishable from that of the wild-type (Figure 4A). *ser-2* null-mutant worms possibly exhibit altered multisensory decision balance, although not statistically distinguishable from the wild-type in our assays. *ser-2* null-mutant worms also exit the 3 M fructose ring in the absence of food odor more readily than wild-type, which could potentially be explained by previously described defects in avoidance and turning behaviors (Donnelly et al., 2013; Rex et al., 2004) (Figure 4A). Unlike the other tyramine receptor null-mutant worms, however, *tyra-2* null-mutant worms readily exit a 3 M ring to approach the source of food odor, phenocopying both *pdf-2* and *tdc-1* null-mutant worms (Figure 4A). Like *pdf-2* and *tdc-1* null-mutant worms, *tyra-2* null-mutant worms are unaffected in the unisensory avoidance-only context (Figure 4A). Furthermore, double null-mutant *pdf-2; tyra-2* worms behave identically to both *pdf-2* and *tyra-2* single-mutant worms, suggesting that these signaling modules operate in the same functional pathway to determine threat-reward decision balance (Figure 4A). Little is known about *tyra-2* function (Donnelly et al., 2013; Jin et al., 2016; Pirri et al., 2009; Rex et al., 2005), and our results now demonstrate that TYRA-2 is the receptor through which tyramine secreted by RIM controls threat-reward decision making.

*tyra-2* is expressed in a number of sensory neurons, including the osmosensory neuron ASH (Rex et al., 2005). Re-expression of *tyra-2* using either of two cell-specific promoters whose expression overlaps only in ASH rescues the wild-type decision balance in *tyra-2* null-mutant worms, while re-expression using a promoter active in other sensory neurons but not ASH has no effect (Figure 4B). Functional imaging of ASH $Ca^{2+}$ responses to osmotic stimuli revealed that exogenous tyramine pre-treatment increases ASH osmosensitivity, indicating neuronal activation (Figure 4C, D, E) (Zahratka et al., 2015). Tyramine potentiation of ASH osmosensitivity is abolished in *tyra-2* null-mutant worms (Figure 4F, G, H). Finally, we compared the time it takes *tyra-2* null-mutant worms to exit the ring in the standard multisensory assay and a time-shifted configuration in which the fructose ring is allowed five extra minutes to diffuse before the worms are placed (Figure S3A). Worm begin

to exit the time-shifted configuration immediately after being placed, while worms begin to exit in the standard assay about five minutes after being placed (Figure S3B, S3C). Therefore exiting in the threat-reward decision assay is determined by the state of the osmotic barrier as each worm confronts it and the osmosensitivity of the ASH neuron as regulated by tyraminergic feedback (Figure S3B, S3C, S3D). As RIM does not form synapses onto ASH (although ASH does synapse onto RIM) (White et al., 1986), taken together these results demonstrate that RIM controls multisensory threat-reward decision making by secreting tyramine to act extrasynaptically at a distance directly on ASH through TYRA-2 to potentiate ASH sensitivity to osmotic stimuli.

## Computational modeling predicts slow, non-linear tyramine regulation of threat-reward decision making

To characterize the interplay between neural activity, neuromodulatory activity, behavior, and the environment, we modeled each of these dynamic components *in silico*. Model worms contain a highly simplified minimal nervous system sufficient for decision making (Figure 5A; see **Experimental Procedures** and Supplemental Methods for details). Model parameters were fit to match the experimental exiting rates of Figure 2B. To illustrate the temporal evolution of the decision process, we plotted the locomotor trajectories and neural and neuromodulatory activity underlying the behavior of example simulated wild-type and *tyra-2* null-mutant worms (Figure 5C, D). This reveals that oscillatory changes in fructose and diacetyl concentration experienced by the worm as it undulates within the arena (Figure 5C) induce corresponding oscillatory changes in the activity of AWA, ASH, and RIM (Figure 5D) that are phase locked to the undulatory locomotor DMN-VMN pattern generator. In both wild-type and *tyra-2* null-mutant worms, the magnitude of RIM and ASH oscillatory activity is larger than the AWA signal, and decreases over time. However, the magnitude of this oscillatory activity in RIM and ASH is higher in wild-type worms than in *tyra-2* null-mutant worms (Figure 5D, S4B, S4C). Furthermore, in virtual *tyra-2* null-mutant worms, the magnitude of RIM and ASH activity decreases over the course of the simulation until it matches AWA activity, which permits exiting of the ring. After exiting, the AWA signal dominates, ASH becomes silent, and RIM becomes inhibited as the worm continuously ascends the diacetyl gradient (Figure 5D). The model thus predicts that RIM activity engages the RIM-ASH feedback loop, thereby decreasing threat tolerance and preventing exiting of the ring (Figure 5D). Importantly, the model also requires a non-linear threshold for RIM activation to trigger tyramine signaling to ASH and slow kinetics of accumulation and decay of the tyramine signal on a timescale of minutes to preclude exiting of wild-type worms even as the fructose barrier continues to diffuse and weaken (Figure 5D, S4D). The reduced activation of ASH and RIM in simulated *tyra-2* null-mutant worms, in which tyraminergic RIM-ASH feedback is absent, encodes increased threat tolerance underlying increased propensity to exit the ring (Figure 5D). Our computational model thus suggests that the slow, continuous, and self-reinforcing enhancement of RIM and ASH activity by top-down tyraminergic positive feedback determines threat tolerance that ultimately controls the decision balance.

## RIM-ASH positive feedback underlies modulation of the threat-reward decision by internal hunger state

Food deprivation increases threat tolerance in the multisensory decision paradigm (Figure 1D). We hypothesized it does so by suppressing RIM activity and thus the RIM-ASH tyraminergic feedback pathway. As a first test of this hypothesis, we examined the effect of food deprivation on *tyra-2* null-mutant worms. In contrast to wild-type worms, *tyra-2* null-mutant worms fail to increase exiting after one hour of food deprivation, and rather maintain their already elevated threat tolerance (Figure 6A). This is consistent with the hypothesis that one hour of food deprivation increases threat tolerance by suppressing tyraminergic RIM-ASH feedback, with *tyra-2* null-mutant worms failing to increase exiting because the RIM-ASH pathway is already fully suppressed. We also measured the effects of food deprivation on unisensory osmotic avoidance. We found that *tyra-2* null-mutant worms deprived of food for one hour exit more readily in the unisensory context, while wild-type worms are still retained (Figure 6B). This result also supports our model that food deprivation suppresses RIM activity and thus tyraminergic RIM-ASH feedback. In our model, RIM inhibition induced by food deprivation disinhibits forward command interneurons and reduces activation of backward command interneurons. This renders retreat from the osmotic ring reliant upon RIM-ASH positive feedback in this context. Five hours of food deprivation further increases exiting of *tyra-2* null-mutant worms in the multisensory context, as seen in wild-type worms (Figure 6A). In the unisensory context, five hours of food deprivation further also increases exiting of both wild-type and *tyra-2* null-mutant worms (Figure 6B). These effects of more extended food deprivation on *tyra-2* null-mutant worms indicate the involvement of RIM-ASH-independent pathways for hunger-dependent increases in threat tolerance. Next we measured the effects of food deprivation on unisensory attraction to food odor. We found that both wild-type and *tyra-2* null-mutant worms exhibit enhanced chemotaxis to diacetyl after one or five hours of food deprivation (Figure 6C, S5). While increased chemotaxis to diacetyl in hungry wild-type and *tyra-2* null-mutant worms could be driven by increased diacetyl sensitivity (Ryan et al., 2014), it is more likely that food deprivation increases attraction to diacetyl by effects on locomotion that result from suppressed RIM activity (Gordus et al., 2015; Gray et al., 2005).

To further test the hypothesis that food deprivation inhibits RIM, we turned to our computational model. We simulated food deprivation as duration-dependent tonic inhibition of RIM, keeping all other model parameters unchanged. We modeled one hour of food deprivation as RIM inhibition of ~0.03 (in arbitrary units), because this level of RIM inhibition increases exiting of simulated wild-type worms to 50%, the same as real worms food-deprived for one hour (compare Figure 6A with Figure 6D). As RIM inhibition increases from 0 to ~0.03, simulated wild-type worms increase exiting more steeply than *tyra-2* null-mutant worms (Figure 6D, Figure S4E, S4F, see Supplemental Movie 1). This qualitatively recapitulates the multisensory experimental results (Figure 6A). In the unisensory fructose-only context, as RIM inhibition increases from 0 to ~0.03, simulated wild-type worms increase exiting less steeply than *tyra-2* null-mutant worms (Figure 6E). This qualitatively recapitulates the unisensory experimental results (Figure 6B). We note that model parameters were selected solely to match simulated exiting rates (Figure 5B) to experimental exiting rates of non-food-deprived worms (Figure 2B), without any

consideration of the effects of food deprivation. Nonetheless, the qualitative recapitulation of experimental effects of increasing food deprivation in both unisensory and multisensory contexts by simulating increasing inhibition of RIM strongly reinforce the conclusion that food deprivation increases threat tolerance by inhibiting RIM and thereby suppressing RIM-ASH tyraminergic feedback.

### Tyramine supplementation and direct inhibition of RIM each recapitulate hunger state modulation of the threat-reward decision *via* RIM-ASH positive feedback

The results presented thus far support a model in which food deprivation increases threat tolerance by inhibiting RIM and thereby suppressing RIM-ASH tyraminergic feedback. To provide additional experimental tests of this model, we directly manipulated neural activity within the circuit. To exogenously induce tyraminergic potentiation of ASH, we added tyramine to the assay plate. Our model predicts that exogenous tyramine will increase threat sensitivity and thereby promote retreat from the ring in multisensory contexts *via tyra-2* (Figure 7A). Exogenous tyramine has no effect on wild-type worms, which already exhibit maximum threat sensitivity (Figure 7B). In contrast, exogenous tyramine suppresses exiting of *tdc-1* null-mutant worms exiting to wild-type levels (Figure 7B). Importantly, the effect of exogenous tyramine is completely eliminated in *tyra-2* null-mutant worms (Figure 7B). We next tested the effect of exogenous tyramine on wild-type worms food-deprived for one hour. Our model predicts that one-hour food deprivation increases exiting *via* suppression of RIM-ASH tyraminergic feedback; therefore, the presence of tyramine, regardless of the worm's internal state, should suppress exiting. Indeed, wild-type worms food-deprived for one hour behave like sated worms in the presence of exogenous tyramine (Figure 7C). Again, *tyra-2* null-mutant worms are unaffected (Figure 7C). Tyramine supplementation completely reverses increased exiting of one-hour food-deprived wild-type worms, thus further indicating that suppression of RIM-ASH tyraminergic feedback underlies increased threat tolerance of hungry worms.

Complementarily, our model predicts that direct inhibition of RIM activity should increase exiting (Figure 7D). Transgenic expression of a histamine-gated chloride channel (His-Cl) specifically in RIM allows for controlled silencing of RIM contingent upon the presence of exogenously applied histamine, as worms do not endogenously use histamine as a neurotransmitter (Pokala et al., 2014). In the absence of exogenous histamine, worms expressing His-Cl in RIM behave like wild-type worms and fail to exit the ring (Figure 7E). Direct inhibition of RIM by addition of 10 mM histamine to the assay plate increases exiting to ~50%, identical to the behavior of *tdc-1* and *tyra-2* null-mutant worms (Figure 7E). Inhibition of RIM by addition of 30 mM histamine to the plate did not increase exiting any further (Figure 7E). Therefore while the absolute level to which RIM is inhibited by histamine is unknown, activation of His-Cl and histamine-mediated inhibition of RIM are apparently saturated by 10 mM histamine. Our model predicts that one hour of food deprivation increases exiting by inhibiting RIM activity; therefore, as with *tyra-2* null-mutant worms, no further increase in exiting of hungry worms is predicted when RIM is directly inhibited. In the absence of histamine, like wild-type worms, worms expressing His-Cl in RIM increase exiting after one hour of food-deprivation (Figure 7F). As predicted by our model, direct inhibition of RIM with histamine has no further effect on exiting of these

one-hour food-deprived worms (Figure 7F). Taken together, these effects of exogenous tyramine and direct inhibition of RIM demonstrate that suppression of RIM-ASH tyraminergic feedback through RIM inhibition quantitatively accounts for the entirety of increased threat tolerance induced by one hour of food deprivation.

## DISCUSSION

Here we demonstrate that tyraminergic RIM-ASH positive feedback controls multisensory threat-reward decision making in *C. elegans*. PDFR-1 activation by PDF-2 in RIM (Figure 2, 3) and extrasynaptic tyraminergic potentiation of ASH (Figure 4) set the decision balance between retreat from an osmotic threat and approach to food odor. We devised a minimal computational neural network model to recapitulate the decision *in silico*. Our model predicts that integration of multisensory inputs in RIM nonlinearly determines the magnitude of the tyramine feedback signal. Using this model, we simulated the dynamic changes in neural and neuromodulatory activity that occur in freely moving worms during decision making, and determined the slow timescale at which RIM-ASH tyraminergic feedback must act to implement the decision (Figure 5, S4D). Our experimental and computational results establish that food deprivation increases threat tolerance through suppression of RIM-ASH positive feedback by inhibition of RIM (Figure 6, 7, S4E, S4F). These studies provide an integrated neuroendocrine circuit architecture for internal state control of multisensory threat-reward decision making.

Tyramine secreted by RIM regulates multisensory decision making by modulating ASH sensitivity extrasynaptically at a distance. Interestingly, our modeling studies predict that the extrasynaptic tyramine signal must both accumulate and decay slowly, modulating ASH sensitivity over long time-scales of multiple minutes in order to appropriately implement the threat-reward decision balance. The computational model is agnostic as to how the slow kinetics of tyramine signaling are implemented. We propose that this slow tyramine signaling functions as a form of memory for the worm by suppressing sensory adaptation to dangerous stimuli sensed over time, a feature which could be advantageous for worms navigating changing environmental conditions. Slow-acting diffusion and accumulation of extrasynaptic signals that act at a distance like tyramine are likely better suited for this purpose than more fast-acting synaptic signals. In addition, tyraminergic RIM-ASH positive feedback could determine the worm’s tolerance to a variety of threats, as the ASH neuron is polymodal and senses multiple noxious cues (Hilliard et al., 2005; Kaplan and Horvitz, 1993).

We conclusively demonstrate that suppression of RIM-ASH tyraminergic feedback through RIM inhibition quantitatively accounts for the entirety of increased threat tolerance induced by one hour of food deprivation. Our studies indicate that RIM is a metabolic modulator of threat-reward decision making. Interestingly, we found that the direct synaptic connections that RIM forms with downstream command locomotor interneurons driving basic attraction and aversion behaviors are dispensable for modulation of threat-reward decision-making. In the decision studied here, the only function of RIM is to provide tyraminergic feedback to ASH based on metabolic state. Extended food deprivation beyond one hour then recruits other currently unknown RIM-ASH-independent pathways for hunger-dependent increases

in threat tolerance. It was recently shown that in RIM and RIC, expression of NKAT-1, an enzyme in the biosynthetic pathway of kynurenic acid, a metabolite whose levels vary with hunger state, underlies hunger modulation of feeding rate (Lemieux et al., 2015). This provides a potential cellular mechanism linking organismic metabolic state to RIM excitability, thereby controlling tyramine secretion, and thus determines the likelihood of exiting the ring during the decision task.

Cell-specific rescue and t-PDF-2 expression experiments support the existence of a PDF-2-PDFR-1 autocrine loop in RIM. Interestingly, autocrine PDF signaling also occurs in the *Drosophila* circadian control network (Choi et al., 2012). Activation of autocrine positive feedback loops, however, are probably not easily reversible – therefore, it is likely that these cascades are only initiated beyond a threshold level of activation modulated by externally derived signals or internal cellular state. Such a mechanism would reinforce the stability of distinct, long-lasting behavioral states, such as behaviors relevant to night versus day, or, in this case, biasing threat-reward decision making in the threat-tolerant or threat-sensitive directions. Therefore, we propose that by flipping a potentially stable switch, the PDF-2-PDFR-1 autocrine loop biases the worm towards threat-sensitive decisions and importantly, eliminates ambivalence when confronted with various situations.

How does RIM-ASH positive feedback control threat-reward decision making? The worm sensory interneuron network downstream of primary sensory neurons captures multisensory information (Ishihara et al., 2002; Luo et al., 2014; Shinkai et al., 2011), and RIM is downstream of this network (Gordus et al., 2015; Guo et al., 2009; Piggott et al., 2011; White et al., 1986). Thus we propose that RIM excitability is set by PDF-2-PDFR-1 autocrine loop activity, and RIM activity fluctuates dynamically as it responds to specific combinations of diacetyl and osmotic stimuli as the worm navigates the decision arena. Ultimately, the worm makes a probabilistic choice between retreat and exit based on the stochastic, instantaneous activity state of RIM, with stochasticity of RIM activity having been previously observed (Gordus et al., 2015). Longer time-scale tyraminergic feedback increases the probability that instantaneous RIM, and therefore ASH, activity states are high. Thus by acutely modifying forward and backward locomotor-control neuron activity through feedforward channels or, on longer time scales, indirectly through tyraminergic RIM-ASH feedback, RIM activity transforms multisensory inputs into a motor decision (Figure S6).

As discussed previously, in human beings and other mammals, a key feature of multisensory integration is internal-state-dependent “top-down” control of perception (Manita et al., 2015; Talsma et al., 2010) by higher-order brain regions (Fairhall and Macaluso, 2009; Fu et al., 2014; Zhang et al., 2014). Interestingly, in the human brain, aminergic neuromodulatory systems like locus ceoruleus are involved in directing attention to food-related cues in a hunger-dependent manner (Mohanty et al., 2008). However, analysis of neural mechanisms in the context of an approach-avoidance decision in human and mammalian systems are limited by technical constraints. Here we describe an integrated circuit that demonstrates a mechanism by which internal physiological hunger state drives a shift in the decision balance of approach and avoidance. The molecular, cellular, and network motifs described here in the worm may be relevant in more complex nervous systems.

## EXPERIMENTAL PROCEDURES

All *C. elegans* strains were maintained on Nematode Growth Medium (NGM) agar plates with *E. coli* OP50 as a food source. Transgenic strains were constructed by injection of plasmid DNA into the germline using standard methods. At least three independent lines were generated, tested, and results aggregated for each transgene.

### Behavioral assays

For unisensory and multisensory assays, 10μL of fructose solution is applied in a 1cm diameter ring centered on a standard NGM plate (Culotti and Russell, 1978). For multisensory assays, 1μL diluted diacetyl was applied to each side of the plate, at least 1cm from the ring border. Ten (unless otherwise indicated) adult worms were transferred inside the ring. Fifteen minutes later, the number of worms outside the ring were counted. For the food deprivation assays, worms were transferred inside the ring from another plate, where they were kept without food for the indicated time interval. For this and other assays, see Supplemental Experimental Procedures for more information. At least five independent assays were performed for each condition. One- or two-way ANOVA, as appropriate, was used to analyze statistical differences, with *post-hoc* Tukey-Kramer tests performed for pairwise comparisons between all pairs of genotypes. We did not include all previously tested genotypes/conditions each time a new genotype/condition was tested. Therefore identical data was presented in multiple figure panels.

### Imaging

Calcium imaging of ASH neurons was performed on young adult worms immobilized in an olfactory chamber as described previously (Chronis et al., 2007). Imaged animals expressed the genetically-encoded calcium sensor GCaMP3 from the *sra-6* promoter (Tian et al., 2009). Prior to loading into the olfactory chamber worms were bathed in neuronal buffer for 10 min either in the presence or absence of 50mM tyramine. Animals were exposed to the test stimulus for 20 sec. Averaged fluorescence was calculated for a region of interest (ROI) surrounding the ASH soma. The percent change in fluorescence for each frame was calculated relative to the corrected fluorescence of the ROI just prior to stimulus onset. See Supplemental Experimental Procedures for more details.

### Computational model

Model animals possess a simplified nervous system comprising sensory neurons AWA and ASH, interneuron RIM, and two reciprocally inhibited motor neurons denoted DMN and VMN, which activate dorsal and ventral body bends, respectively. AWA and ASH sensory neurons respond with transient activation to changes in diacetyl or fructose stimuli, respectively. Activation of model sensory neurons AWA and ASH provides differentially weighted inhibitory and excitatory inputs onto RIM, respectively. RIM integrates these sensory inputs and inhibits motorneurons DMN and VMN to bias dorsal versus ventral bends, thereby inducing gradual steering of the worm. Additionally, RIM activity positively increases the likelihood of pirouettes, which are modeled as instantaneous step changes in angular heading. The simulation also includes RIM-ASH tyraminergic positive feedback. Tyraminergic potentiation of ASH in the model is only engaged above a threshold level of

RIM activation. *tyra-2* null-mutant worms are modeled as lacking this tyraminergic feedback to ASH. Model parameters were manually calibrated until exiting rates of simulated wild-type and *tyra-2* null-mutant worms matched experimental exiting rates in multisensory and unisensory contexts for 2 M, 3 M, and 4 M fructose. The virtual decision arena comprises a continuously diffusing fructose gradient ring and time-invariant diacetyl gradients originating from two spots outside the ring. Each simulation begins with a single worm in the center of the virtual arena with a randomly selected initial heading, and the simulation is allowed to proceed for fifteen virtual minutes. See Supplemental Experimental Procedures for additional details.

## Supplementary Material

Refer to Web version on PubMed Central for supplementary material.

## Acknowledgments

We thank S. Mitani, C. Bargmann, and the Caenorhabditis Genetics Center for strains, K. Ashrafi, A. Maricq, C. Rankin, D. Colon-Ramos, M. Chalfie for cell-specific promoter reagents, M. Hammarlund for other vectors, V. Reinke for assistance and advice, G. Jansen for sharing unpublished data, assistance and advice in generating the computational model, S. Braunstein, members of the Cohen, Koelle, and Nitabach labs and the Yale worm community for technical advice and comments, and Daeyeol Lee and Leslie Vosshall for comments on the manuscript. D.D.G was supported by a National Institute of Neurological Disease and Stroke (NINDS) National Institutes of Health (NIH) Predoctoral Fellowship (F31NS080628). Work in the laboratory of M.N.N. was supported in part by NINDS, NIH (R01NS055035, R01NS056443, R01NS091070) and National Institute of General Medical Sciences, NIH (R01GM098931). M.R.K. was supported by NINDS, NIH (R01NS036918). N.C. and T.S. were supported by the Engineering and Physical Sciences Research Council (EPSRC, EP/J004057/1). Computational work was undertaken on ARC2 and MARC1 (High Performance Computing facilities, University of Leeds). MARC1 was funded by the Leeds Institute for Data Analytics.

## References

Alkema MJ, Hunter-Ensor M, Ringstad N, Horvitz HR. Tyramine Functions independently of octopamine in the Caenorhabditis elegans nervous system. Neuron. 2005; 46:247–260. [PubMed: 15848803]

Barrios A, Ghosh R, Fang C, Emmons SW, Barr MM. PDF-1 neuropeptide signaling modulates a neural circuit for mate-searching behavior in C. elegans. Nature neuroscience. 2012; 15:1675–1682. [PubMed: 23143519]

Berthoud HR. Metabolic and hedonic drives in the neural control of appetite: who is the boss? Curr Opin Neurobiol. 2011; 21:888–896. [PubMed: 21981809]

Choi C, Cao G, Tanenhaus AK, McCarthy EV, Jung M, Schleyer W, Shang Y, Rosbash M, Yin JC, Nitabach MN. Autoreceptor control of peptide/neurotransmitter corelease from PDF neurons determines allocation of circadian activity in drosophila. Cell Rep. 2012; 2:332–344. [PubMed: 22938867]

Choi C, Fortin JP, McCarthy E, Oksman L, Kopin AS, Nitabach MN. Cellular dissection of circadian peptide signals with genetically encoded membrane-tethered ligands. Current biology : CB. 2009; 19:1167–1175. [PubMed: 19592252]

Choi S, Chatzigeorgiou M, Taylor KP, Schafer WR, Kaplan JM. Analysis of NPR-1 reveals a circuit mechanism for behavioral quiescence in C. elegans. Neuron. 2013; 78:869–880. [PubMed: 23764289]

Chronis N, Zimmer M, Bargmann CI. Microfluidics for in vivo imaging of neuronal and behavioral activity in Caenorhabditis elegans. Nature methods. 2007; 4:727–731. [PubMed: 17704783]

Culotti JG, Russell RL. Osmotic avoidance defective mutants of the nematode Caenorhabditis elegans. Genetics. 1978; 90:243–256. [PubMed: 730048]

Donnelly JL, Clark CM, Leifer AM, Pirri JK, Haburcak M, Francis MM, Samuel AD, Alkema MJ. Monoaminergic orchestration of motor programs in a complex C. elegans behavior. PLoS biology. 2013; 11:e1001529. [PubMed: 23565061]

Fairhall SL, Macaluso E. Spatial attention can modulate audiovisual integration at multiple cortical and subcortical sites. Eur J Neurosci. 2009; 29:1247–1257. [PubMed: 19302160]

Flavell SW, Pokala N, Macosko EZ, Albrecht DR, Larsch J, Bargmann CI. Serotonin and the neuropeptide PDF initiate and extend opposing behavioral states in C. elegans. Cell. 2013; 154:1023–1035. [PubMed: 23972393]

Fortin JP, Zhu Y, Choi C, Beinborn M, Nitabach MN, Kopin AS. Membrane-tethered ligands are effective probes for exploring class B1 G protein-coupled receptor function. Proceedings of the National Academy of Sciences of the United States of America. 2009; 106:8049–8054. [PubMed: 19416829]

Frezal L, Felix MA. C. elegans outside the Petri dish. Elife. 2015:4.

Fu Y, Tucciarone JM, Espinosa JS, Sheng N, Darcy DP, Nicoll RA, Huang ZJ, Stryker MP. A cortical circuit for gain control by behavioral state. Cell. 2014; 156:1139–1152. [PubMed: 24630718]

Gordus A, Pokala N, Levy S, Flavell SW, Bargmann CI. Feedback from network States generates variability in a probabilistic olfactory circuit. Cell. 2015; 161:215–227. [PubMed: 25772698]

Gray JM, Hill JJ, Bargmann CI. A circuit for navigation in Caenorhabditis elegans. Proceedings of the National Academy of Sciences of the United States of America. 2005; 102:3184–3191. [PubMed: 15689400]

Guo ZV, Hart AC, Ramanathan S. Optical interrogation of neural circuits in Caenorhabditis elegans. Nature methods. 2009; 6:891–896. [PubMed: 19898486]

Hilliard MA, Apicella AJ, Kerr R, Suzuki H, Bazzicalupo P, Schafer WR. In vivo imaging of C. elegans ASH neurons: cellular response and adaptation to chemical repellents. The EMBO journal. 2005; 24:63–72. [PubMed: 15577941]

Ishihara T, Iino Y, Mohri A, Mori I, Gengyo-Ando K, Mitani S, Katsura I. HEN-1, a secretory protein with an LDL receptor motif, regulates sensory integration and learning in Caenorhabditis elegans. Cell. 2002; 109:639–649. [PubMed: 12062106]

Janssen T, Husson SJ, Lindemans M, Mertens I, Rademakers S, Ver Donck K, Geysen J, Jansen G, Schoofs L. Functional characterization of three G protein-coupled receptors for pigment dispersing factors in Caenorhabditis elegans. The Journal of biological chemistry. 2008; 283:15241–15249. [PubMed: 18390545]

Janssen T, Husson SJ, Meelkop E, Temmerman L, Lindemans M, Verstraelen K, Rademakers S, Mertens I, Nitabach M, Jansen G, et al. Discovery and characterization of a conserved pigment dispersing factor-like neuropeptide pathway in Caenorhabditis elegans. Journal of neurochemistry. 2009; 111:228–241. [PubMed: 19686386]

Jin X, Pokala N, Bargmann CI. Distinct Circuits for the Formation and Retrieval of an Imprinted Olfactory Memory. Cell. 2016; 164:632–643. [PubMed: 26871629]

Jose AM, Bany IA, Chase DL, Koelle MR. A specific subset of transient receptor potential vanilloid-type channel subunits in Caenorhabditis elegans endocrine cells function as mixed heteromers to promote neurotransmitter release. Genetics. 2007; 175:93–105. [PubMed: 17057248]

Kaplan JM, Horvitz HR. A dual mechanosensory and chemosensory neuron in Caenorhabditis elegans. Proceedings of the National Academy of Sciences of the United States of America. 1993; 90:2227–2231. [PubMed: 8460126]

Kawano T, Po MD, Gao S, Leung G, Ryu WS, Zhen M. An imbalancing act: gap junctions reduce the backward motor circuit activity to bias C. elegans for forward locomotion. Neuron. 2011; 72:572–586. [PubMed: 22099460]

Krupp JJ, Billeter JC, Wong A, Choi C, Nitabach MN, Levine JD. Pigment-dispersing factor modulates pheromone production in clock cells that influence mating in drosophila. Neuron. 2013; 79:54–68. [PubMed: 23849197]

Kunst M, Hughes ME, Raccuglia D, Felix M, Li M, Barnett G, Duah J, Nitabach MN. Calcitonin gene-related peptide neurons mediate sleep-specific circadian output in Drosophila. Current biology : CB. 2014; 24:2652–2664. [PubMed: 25455031]

Lemieux GA, Cunningham KA, Lin L, Mayer F, Werb Z, Ashrafi K. Kynurenic acid is a nutritional cue that enables behavioral plasticity. Cell. 2015; 160:119–131. [PubMed: 25594177]

Li Z, Li Y, Yi Y, Huang W, Yang S, Niu W, Zhang L, Xu Z, Qu A, Wu Z, et al. Dissecting a central flip-flop circuit that integrates contradictory sensory cues in C. elegans feeding regulation. Nat Commun. 2012; 3:776. [PubMed: 22491324]

Luo L, Wen Q, Ren J, Hendricks M, Gershow M, Qin Y, Greenwood J, Soucy ER, Klein M, Smith-Parker HK, et al. Dynamic encoding of perception, memory, and movement in a C. elegans chemotaxis circuit. Neuron. 2014; 82:1115–1128. [PubMed: 24908490]

Manita S, Suzuki T, Homma C, Matsumoto T, Odagawa M, Yamada K, Ota K, Matsubara C, Inutsuka A, Sato M, et al. A Top-Down Cortical Circuit for Accurate Sensory Perception. Neuron. 2015

Meelkop E, Temmerman L, Janssen T, Suetens N, Beets I, Van Rompay L, Shanmugam N, Husson SJ, Schoofs L. PDF receptor signaling in Caenorhabditis elegans modulates locomotion and egg-laying. Molecular and cellular endocrinology. 2012; 361:232–240. [PubMed: 22579613]

Mohanty A, Gitelman DR, Small DM, Mesulam MM. The spatial attention network interacts with limbic and monoaminergic systems to modulate motivation-induced attention shifts. Cereb Cortex. 2008; 18:2604–2613. [PubMed: 18308706]

Piggott BJ, Liu J, Feng Z, Wescott SA, Xu XZ. The neural circuits and synaptic mechanisms underlying motor initiation in C. elegans. Cell. 2011; 147:922–933. [PubMed: 22078887]

Pirri JK, McPherson AD, Donnelly JL, Francis MM, Alkema MJ. A tyramine-gated chloride channel coordinates distinct motor programs of a Caenorhabditis elegans escape response. Neuron. 2009; 62:526–538. [PubMed: 19477154]

Pokala N, Liu Q, Gordus A, Bargmann CI. Inducible and titratable silencing of Caenorhabditis elegans neurons in vivo with histamine-gated chloride channels. Proceedings of the National Academy of Sciences of the United States of America. 2014; 111:2770–2775. [PubMed: 24550306]

Rangel A, Camerer C, Montague PR. A framework for studying the neurobiology of value-based decision making. Nat Rev Neurosci. 2008; 9:545–556. [PubMed: 18545266]

Rex E, Hapiak V, Hobson R, Smith K, Xiao H, Komuniecki R. TYRA-2 (F01E11.5): a Caenorhabditis elegans tyramine receptor expressed in the MC and NSM pharyngeal neurons. Journal of neurochemistry. 2005; 94:181–191. [PubMed: 15953361]

Rex E, Komuniecki RW. Characterization of a tyramine receptor from Caenorhabditis elegans. Journal of neurochemistry. 2002; 82:1352–1359. [PubMed: 12354282]

Rex E, Molitor SC, Hapiak V, Xiao H, Henderson M, Komuniecki R. Tyramine receptor (SER-2) isoforms are involved in the regulation of pharyngeal pumping and foraging behavior in Caenorhabditis elegans. Journal of neurochemistry. 2004; 91:1104–1115. [PubMed: 15569254]

Ryan DA, Miller RM, Lee K, Neal SJ, Fagan KA, Sengupta P, Portman DS. Sex, age, and hunger regulate behavioral prioritization through dynamic modulation of chemoreceptor expression. Current biology : CB. 2014; 24:2509–2517. [PubMed: 25438941]

Sengupta P, Chou JH, Bargmann CI. odr-10 encodes a seven transmembrane domain olfactory receptor required for responses to the odorant diacetyl. Cell. 1996; 84:899–909. [PubMed: 8601313]

Shinkai Y, Yamamoto Y, Fujiwara M, Tabata T, Murayama T, Hirotsu T, Ikeda DD, Tsunozaki M, Iino Y, Bargmann CI, et al. Behavioral choice between conflicting alternatives is regulated by a receptor guanylyl cyclase, GCY-28, and a receptor tyrosine kinase, SCD-2, in AIA interneurons of Caenorhabditis elegans. The Journal of neuroscience : the official journal of the Society for Neuroscience. 2011; 31:3007–3015. [PubMed: 21414922]

Solomon A, Bandhakavi S, Jabbar S, Shah R, Beitel GJ, Morimoto RI. Caenorhabditis elegans OSR-1 regulates behavioral and physiological responses to hyperosmotic environments. Genetics. 2004; 167:161–170. [PubMed: 15166144]

Talsma D. Predictive coding and multisensory integration: an attentional account of the multisensory mind. Front Integr Neurosci. 2015; 9:19. [PubMed: 25859192]

Talsma D, Senkowski D, Soto-Faraco S, Woldorff MG. The multifaceted interplay between attention and multisensory integration. Trends in cognitive sciences. 2010; 14:400–410. [PubMed: 20675182]

Tian L, Hires SA, Mao T, Huber D, Chiappe ME, Chalasani SH, Petreanu L, Akerboom J, McKinney SA, Schreiter ER, et al. Imaging neural activity in worms, flies and mice with improved GCaMP calcium indicators. Nature methods. 2009; 6:875–881. [PubMed: 19898485]

Varshney LR, Chen BL, Paniagua E, Hall DH, Chklovskii DB. Structural properties of the Caenorhabditis elegans neuronal network. PLoS Comput Biol. 2011; 7:e1001066. [PubMed: 21304930]

Wang D, Yu Y, Li Y, Wang Y, Wang D. Dopamine receptors antagonistically regulate behavioral choice between conflicting alternatives in C. elegans. PLoS One. 2014; 9:e115985. [PubMed: 25536037]

White JG, Southgate E, Thomson JN, Brenner S. The structure of the nervous system of the nematode Caenorhabditis elegans. Philosophical transactions of the Royal Society of London Series B, Biological sciences. 1986; 314:1–340. [PubMed: 22462104]

Wragg RT, Hapiak V, Miller SB, Harris GP, Gray J, Komuniecki PR, Komuniecki RW. Tyramine and octopamine independently inhibit serotonin-stimulated aversive behaviors in Caenorhabditis elegans through two novel amine receptors. The Journal of neuroscience : the official journal of the Society for Neuroscience. 2007; 27:13402–13412. [PubMed: 18057198]

Zahratka JA, Williams PD, Summers PJ, Komuniecki RW, Bamber BA. Serotonin differentially modulates Ca2+ transients and depolarization in a C. elegans nociceptor. J Neurophysiol. 2015; 113:1041–1050. [PubMed: 25411461]

Zhang S, Xu M, Kamigaki T, Hoang Do JP, Chang WC, Jenvay S, Miyamichi K, Luo L, Dan Y. Selective attention. Long-range and local circuits for top-down modulation of visual cortex processing. Science. 2014; 345:660–665. [PubMed: 25104383]

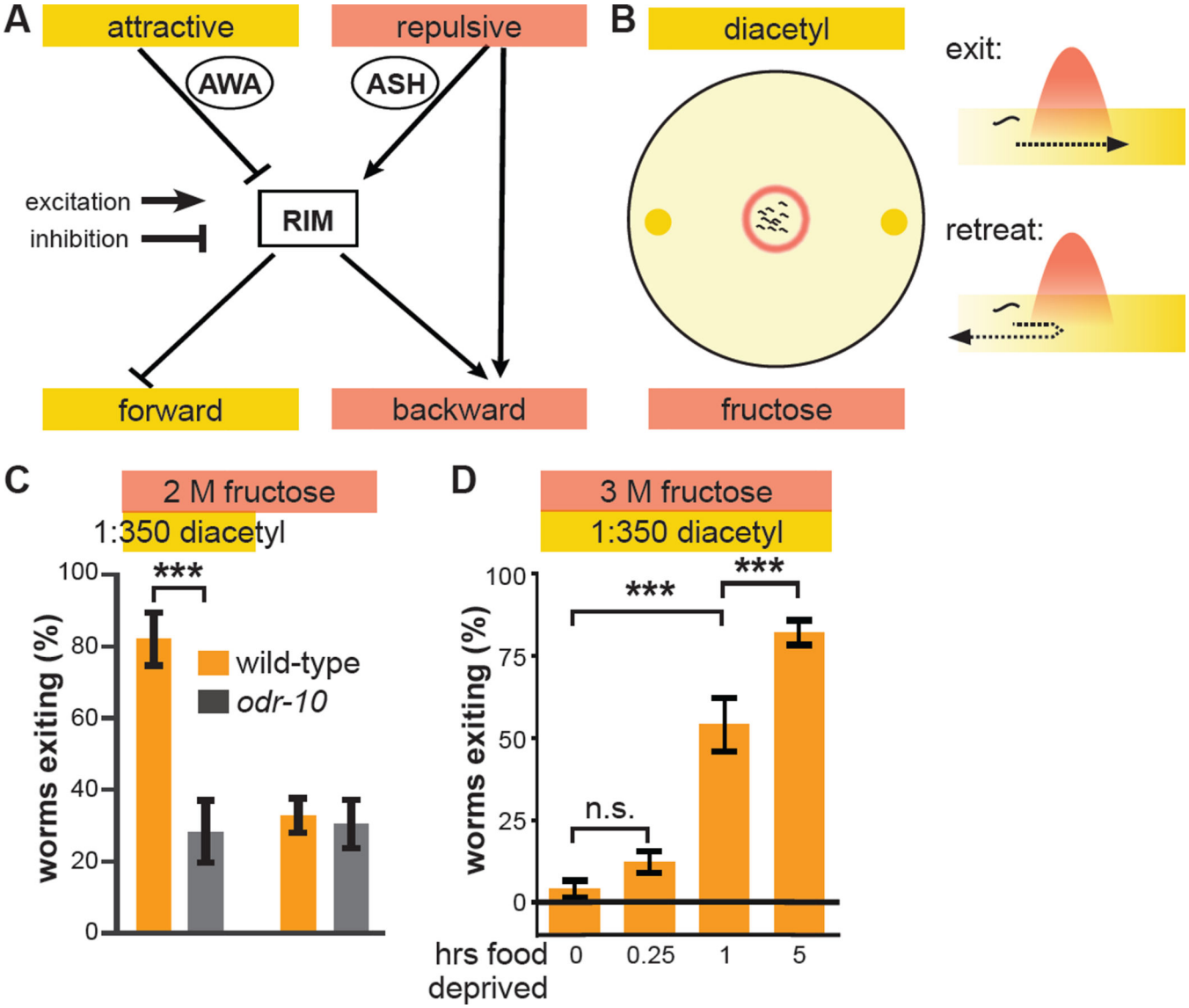


**Figure 1. Hunger state modulates a multisensory threat-reward decision**

**(A)** Schematic of information flow in the *C. elegans* sensorimotor control network. The AWA primary sensory neuron that responds to attractive stimuli like diacetyl food odor indirectly inhibits the RIM interneuron. The ASH primary sensory neuron that responds to aversive stimuli like hyperosmolarity indirectly excites RIM. RIM directly inhibits forward command interneurons and directly excites backward command interneurons to control the balance between forward and backward locomotion. ASH also bypasses RIM to directly excite backward command interneurons.

**(B)** Schematic of the decision making assay. Worms (black squiggles) are placed in the center of a hyperosmotic fructose ring (red circle) with the food odor diacetyl (yellow spots) outside the ring. As each worm ascends the attractive diacetyl gradient, it encounters the aversive hyperosmotic ring, where it either proceeds to exit or retreats to remain in the ring. The decision balance is quantified as the percent of worms that exit the ring during a fifteen minute trial.

**(C)** Wild-type and *odr-10* null-mutant worm tolerance of 2 M fructose ring in presence or absence of food odor. *odr-10* null-mutant worms lack the olfactory receptor that senses diacetyl.

**(D)** Effect of increasing food deprivation on decision to exit a 3 M fructose ring in the presence of food odor.

(Identical data is presented in multiple data sets, as all previously tested genotypes/conditions were not tested every time we extended our analysis to additional genotypes/conditions. Unless otherwise indicated, data in all Figures represent the average of at least five independent assays with ten worms per assay. All statistical comparisons are by one- or two-way ANOVA, as appropriate, with Tukey-Kramer paired-comparison test applied to all pairs of genotypes. Error bars denote s.e.m.; ***, $p < 0.001$.)

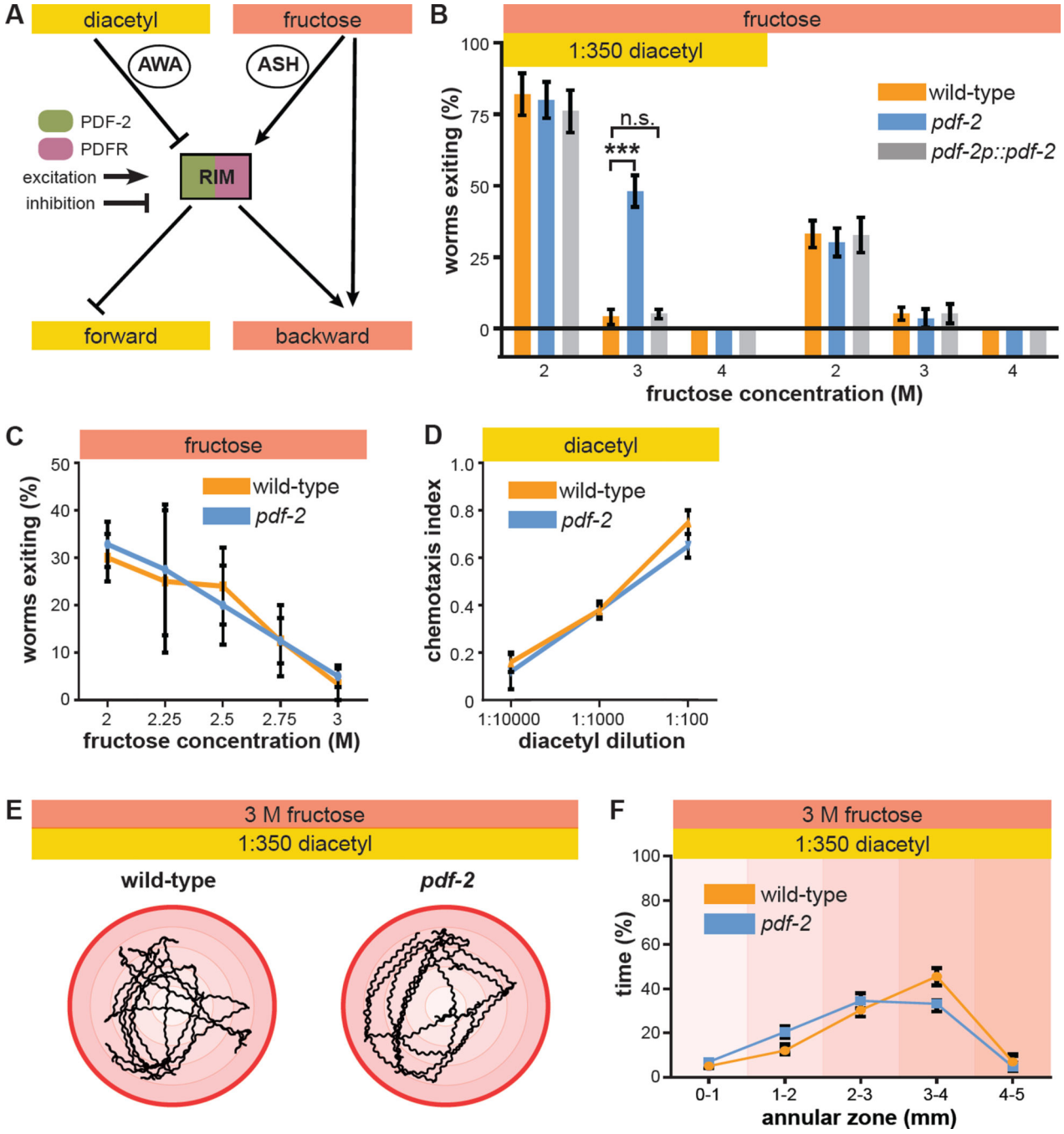


**Figure 2. PDF-2 neuropeptide regulates multisensory decision making**

**(A)** RIM is potentially a peptide-modulated locus for internal state control of threat-reward decision making. RIM expresses both the neuropeptide PDF-2 and its G protein-coupled receptor PDFR-1.

**(B)** Decision balance of wild-type and *pdf-2* null-mutant worms encountering a 2 M, 3 M, or 4 M fructose ring in the presence or absence of food odor. Rescue of *pdf-2* null-mutant phenotype by re-expression of a *pdf-2* transgene under the control of its own promoter.

**(C)** Exiting of the osmotic ring in the absence of food odor in wild-type and *pdf-2* null-mutant worms.

**(D)** Chemotaxis to various concentrations of diacetyl, measured as the fraction of worms that move to a test spot of diacetyl dilution versus a control spot of water after a fifteen minute trial on a standard assay plate, in wild-type and *pdf-2* null-mutant worms.

**(E)** Representative five minute trajectories of wild-type and *pdf-2* null-mutant worms inside a 3 M ring with food odor outside. The outer red circle represents the osmotic ring, and the shading indicates 1mm annular zones.

**(F)** Time spent by wild-type and *pdf-2* null-mutant worms in each of the radial zones ($n$=7–10 worms for each genotype, $F = 1.688$, $p = 0.160$).

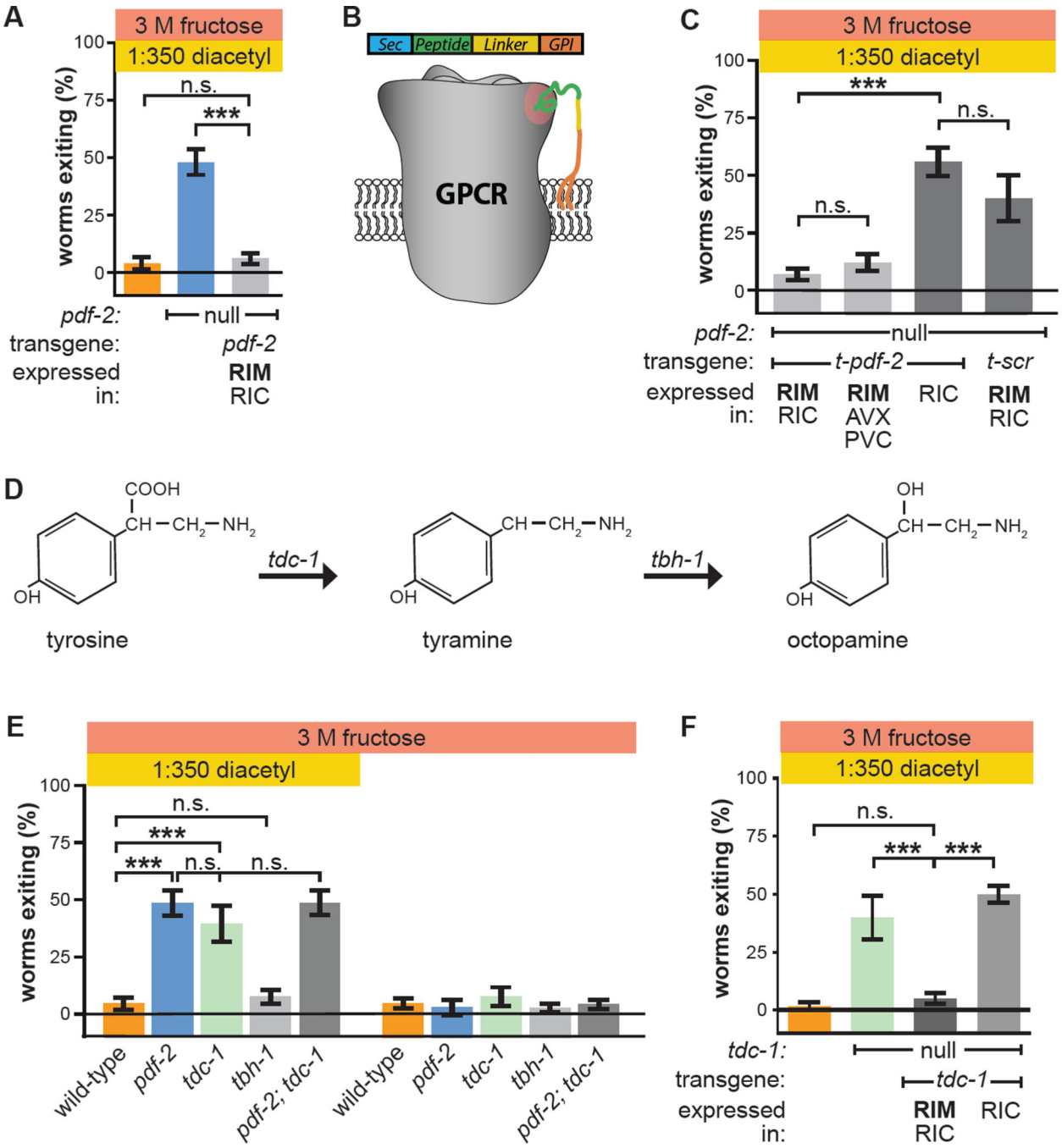


**Figure 3. PDF-2 signaling to PDFR-1 in RIM controls the multisensory decision balance by modulating tyramine secretion**

**(A)** Re-expression of PDF-2 in RIM and RIC in *pdf-2* null-mutant worms using the *tdc-1* promoter.

**(B)** Membrane-tethered peptide (t-peptide) system. Bioactive peptides can be expressed as chimeric fusion proteins with N-terminal secretory signal sequences and C-terminal glycolipid anchor targeting signals. t-peptides are secreted, but remain covalently anchored

to the plasma membrane, and thus only activate their cognate receptors cell-autonomously. Adapted from Choi et al., 2009.

**(C)** Expression in *pdf-2* null-mutant worms of t-PDF-2 using either of two promoters whose activity overlaps only in RIM; expression of t-PDF-2 in RIC alone; or expression of sequence-scrambled t-SCR in RIM and RIC. The *tdc-1, nmr-2*, and *tbh-1* promoters are used to drive expression in RIM and RIC; RIM, multiple AV neurons, and PVC; and RIC alone, respectively.

**(D)** Tyramine is synthesized from tyrosine by tyrosine decarboxylase (TDC), encoded by the *tdc-1* gene expressed in RIM and RIC. Octopamine is synthesized from tyramine by tyramine-β-hydroxylase (TBH), encoded by the *tbh-1* gene expressed in RIC.

**(E)** Multisensory and unisensory decision balance of *tdc-1* null-mutant worms, which lack both tyramine and octopamine, and *tbh-1* null-mutant worms, which lack only octopamine. Decision balance of *pdf-2; tdc-1* double-mutant is also shown.

**(F)** Re-expression of *tdc-1* in RIM and RIC, but not RIC alone, in *tdc-1* null-mutant worms.

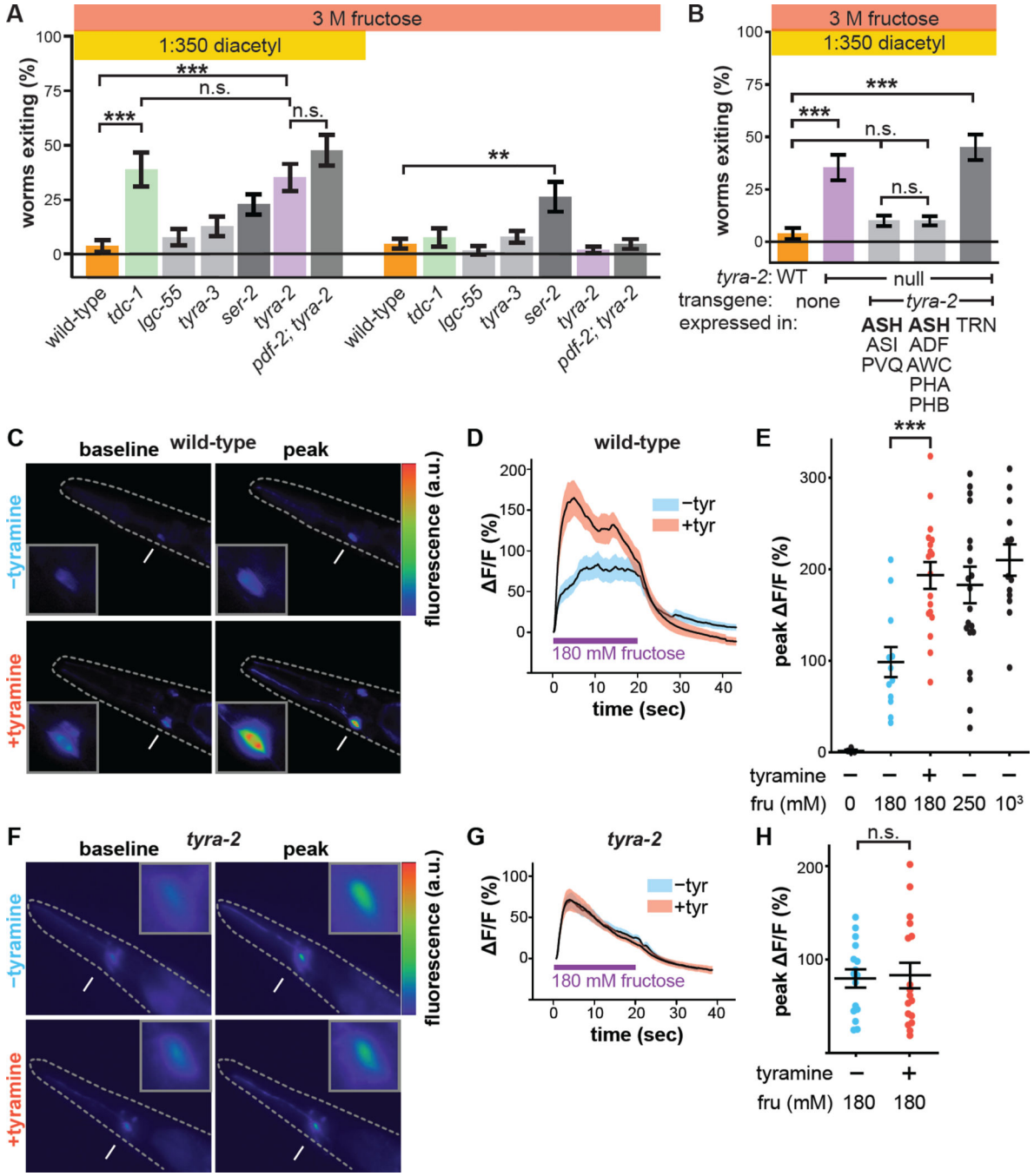


**Figure 4. Tyramine acts on its receptor TYRA-2 in ASH osmosensory neuron to regulate the multisensory decision balance**

**(A)** Multisensory and unisensory decision balance of tyramine receptor mutants. Tyramine GPCR *ser-2* null-mutant worms exhibit increased exiting in both multisensory (*p* vs wild-type = 0.136) and unisensory contexts, though only the increased exiting in the unisensory context is statistically significant compared to wild-type (**, *p* = 0.009). Decision balance of the *pdf-2; tyra-2* double-mutant is also shown.

**(B)** Re-expression of *tyra-2* in *tyra-2* null-mutant worms under the control of the *sra-6* or *gpa-13* promoters, whose activity overlaps solely in ASH. Re-expression of *tyra-2* using the *mec-17* promoter in touch receptor neurons (TRN), some of which also normally express *tyra-2*.

**(C–E)** Representative images (C), time course (D), and peak (E) $Ca^{2+}$ responses of ASH to 180 mM fructose (unless otherwise indicated) in wild-type worms with or without 50 mM tyramine pre-treatment imaged using GCaMP3.

**(F–H)** Representative images (F), time course (G), and peak (H) $Ca^{2+}$ responses of ASH to 180 mM fructose in *tyra-2* null-mutant worms with or without 50 mM tyramine pre-treatment imaged using GCaMP3.

(Arrows indicate ASH cell body, magnified in the insets. Dashed lines outline the worm. mean + s.e.m; circles represent peak responses of individual animals; $n$>12 animals per genotype and treatment condition.)

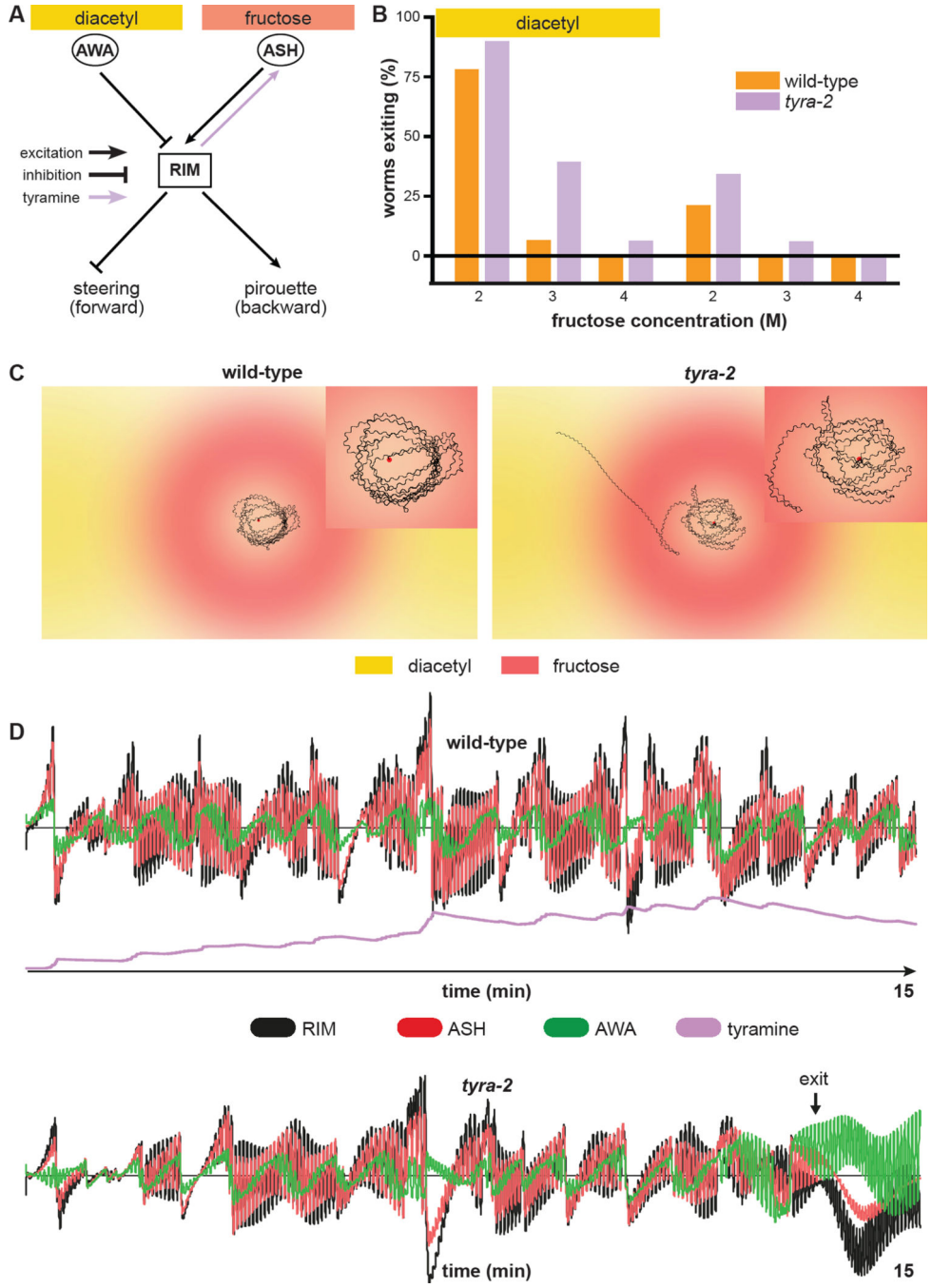


**Figure 5. Computational modeling predicts non-linear slow tyramine signaling by RIM to ASH**

**(A)** Schematic of the simplified nervous system used for computational modeling. AWA and ASH provide direct inhibitory and excitatory inputs onto RIM, respectively. RIM integrates these sensory inputs and directionally biases forward locomotion via inhibition of steering and pirouette modulation. Tyraminergic positive feedback from RIM to ASH increases ASH sensitivity to osmotic stimuli. Simulated *tyra-2* null-mutant worms lack the tyraminergic RIM-ASH signal.

**(B)** Decision balance of simulated wild-type and *tyra-2* null-mutant worms encountering a 2 M, 3 M, or 4 M fructose ring in the presence or absence of food odor. $n$=1000 single worm simulations per genotype and condition.
**(C)** Sample fifteen-minute trajectories of simulated wild-type and *tyra-2* null-mutant worms inside a 3 M ring with food odor outside. Trajectories are magnified in the insets.
**(D)** Neural activity profiles of AWA, ASH, and RIM during the simulated trajectories in (**C**). Activity of individual neurons and of tyramine signals are expressed in arbitrary units, plotted to the same scale for the simulated wild-type and *tyra-2* null-mutant worms.

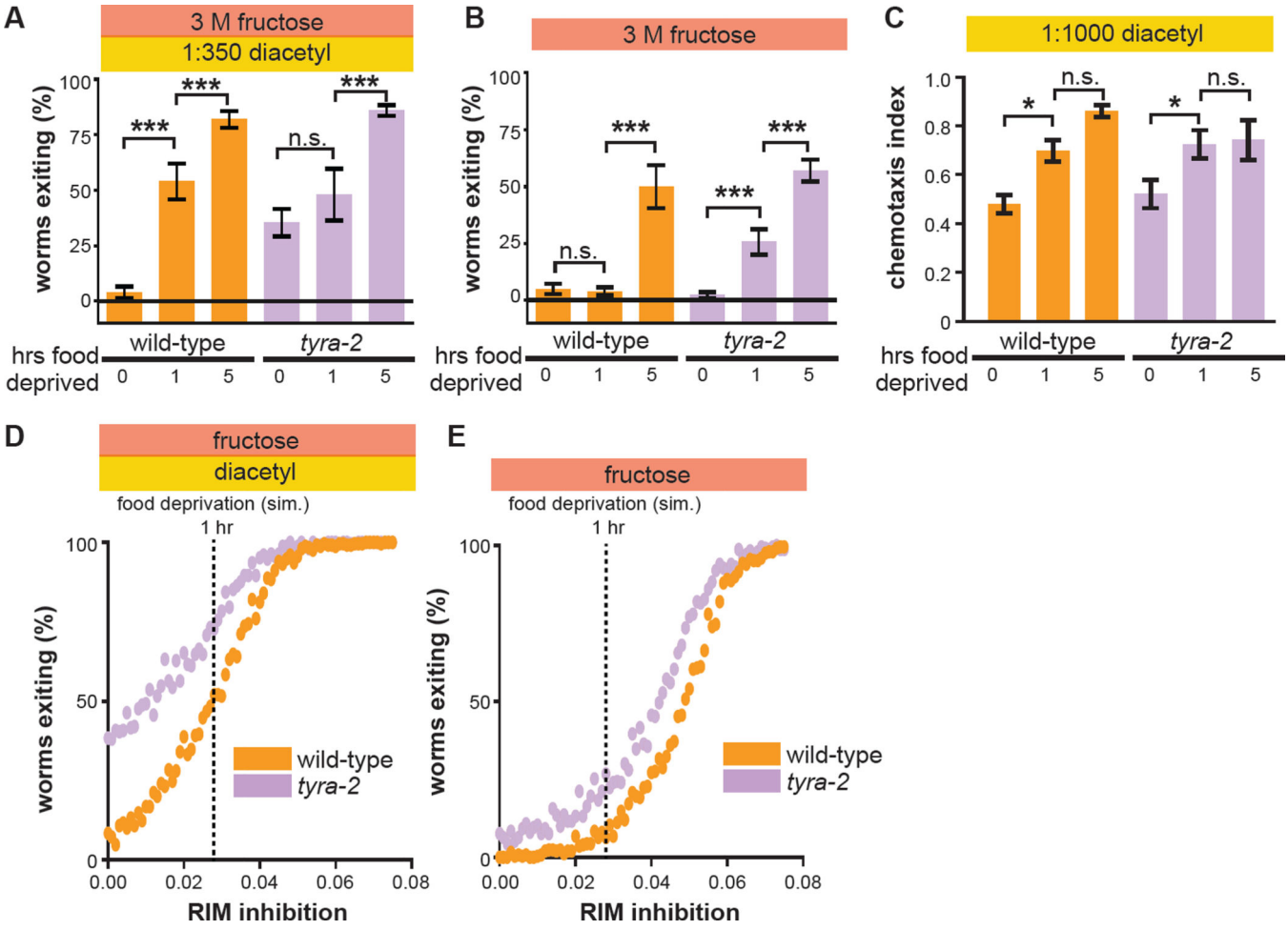


**Figure 6. One-hour food deprivation fails to increase threat tolerance of *tyra-2* null-mutant worms**

**(A–C)** Effect of one hour or five hours of food deprivation on wild-type and *tyra-2* null-mutant worm multisensory decision balance (A), exiting of a 3 M fructose ring in the absence of food odor (B), and chemotaxis to 1:1000 diacetyl (C). (*, $p<0.05$.)

**(D** and **E)** Effect of increasing RIM inhibition on simulated wild-type and *tyra-2* null-mutant worm multisensory (D) or unisensory (E) decision balance. Vertical dashed lines indicate the degree of RIM inhibition that results in exiting rates for simulated wild-type worms that match those of real worms deprived of food for the indicated durations (see panel A). $n$=250 simulated worms for each genotype and strength of RIM inhibition.

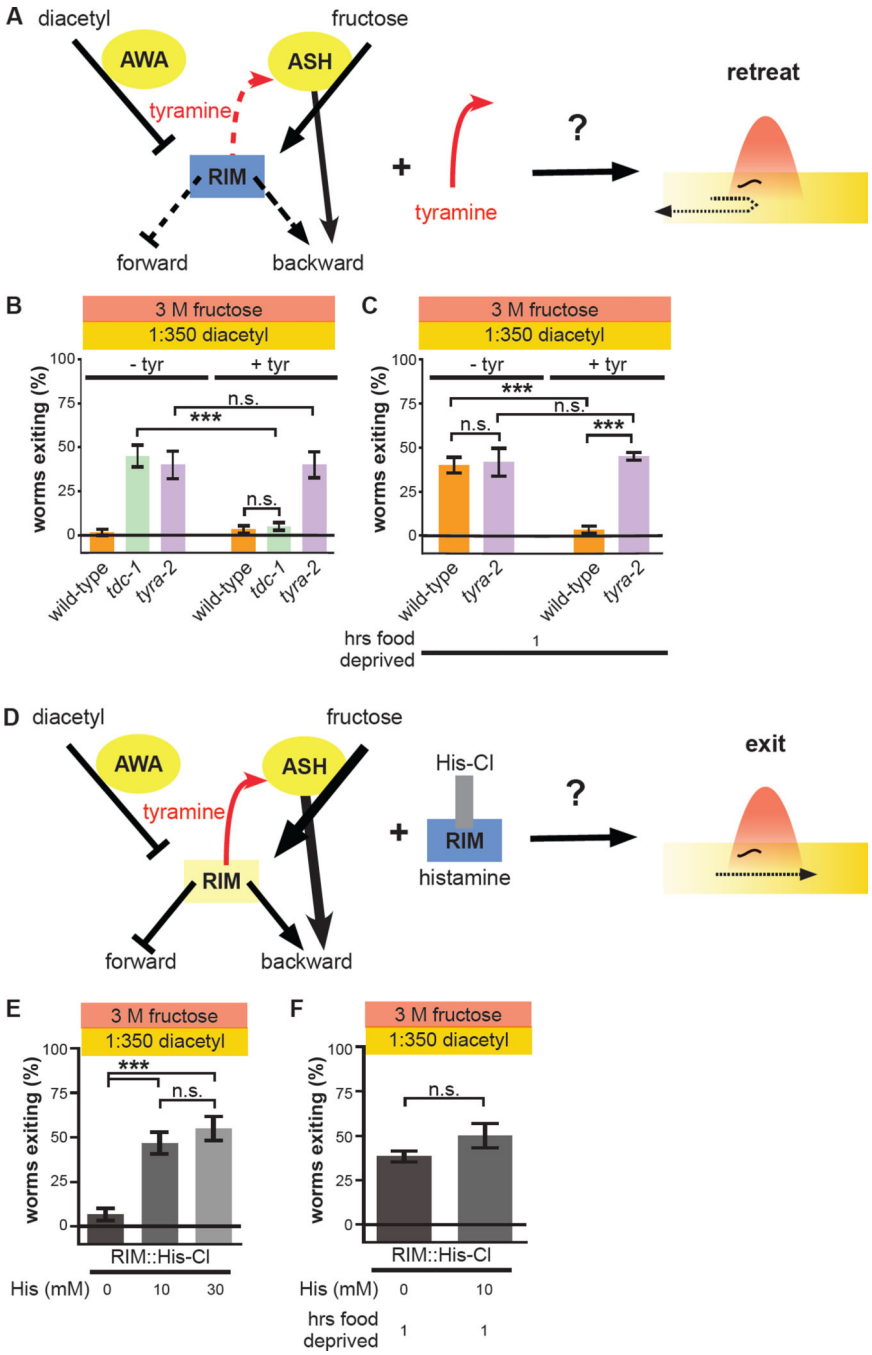


**Figure 7. One-hour food deprivation increases threat tolerance by inhibiting RIM activity and suppressing RIM-ASH tyraminergic potentiation**

**(A)** Schematic depicting prediction that exogenous tyramine increases threat sensitivity. Exogenous tyramine is predicted to reverse the effects of suppression of the RIM-ASH positive feedback loop on threat sensitivity. Yellow represents strong activity, while blue represents weak activity. Thickness of solid lines represents strength of signals, and dashed lines represent inactive signals.

**(B)** Effect of exogenous tyramine on multisensory decisions of wild-type, *tdc-1* null-mutant, and *tyra-2* null-mutant worms.

**(C)** Effect of **e**xogenous tyramine on multisensory decisions of one-hour food-deprived wild-type and *tyra-2* null-mutant worms.

**(D)** Schematic depicting prediction that inhibition of RIM increases threat tolerance. Inhibition of RIM expressing His-Cl with exogenous histamine is predicted to increase threat tolerance and mimic one hour of food deprivation.

**(E)** Effect of 0, 10 mM, and 30 mM histamine on multisensory decision balance of worms expressing RIM::His-Cl.

**(F)** Effect of 0 and 10 mM histamine on multisensory decision balance of one-hour food-deprived worms expressing RIM::His-Cl.